HHS Public Access

Author manuscript

Head Neck. Author manuscript; available in PMC 2018 January 22.

Published in final edited form as:

Head Neck. 2014 September ; 36(9): 1329–1334. doi:10.1002/hed.23452.

Optical coherence tomography imaging during thyroid and parathyroid surgery: A novel system of tissue identification and differentiation to obviate tissue resection and frozen section

Luiz C. Conti de Freitas, MD, PhD[1,2,4], **Eimear Phelan, MD**[1], **Linbo Liu, PhD**[2], **Joseph Gardecki, PhD**[2], **Eman Namati, PhD**[2], **Willian C. Warger, PhD**[2], **Guillermo J. Tearney, MD,PhD**[2], and **Gregory W. Randolph, MD**[1,3,*]

[1]Division of Thyroid and Parathyroid Surgery, Department of Otolaryngology Head and Neck Surgery, Massachusetts Eye and Ear Infirmary, Boston, Massachusetts

[2]Wellman Center of Photomedicine and Department of Pathology, Massachusetts General Hospital, Boston, Massachusetts

[3]Division of Surgical Oncology, Department of Surgery, Massachusetts General Hospital, Boston, Massachusetts

[4]Division of Head and Neck Surgery, Department of Ophthalmology, Otolaryngology, Head and Neck Surgery, Ribeirão Preto Medical School, University of São Paulo, São Paulo, Brazil

Abstract

Background—Optical coherence tomography (OCT) allows tissue histologic-like evaluation, but without tissue fixation or staining. We investigated OCT images from tissues obtained at thyroid and parathyroid surgeries to provide a preliminary assessment as to whether these images contain sufficient information for recognition and differentiation of normal neck tissues.

Methods—Normal tissues were obtained from patients undergoing surgical treatment. Two new-generation OCT systems, including optical frequency domain imaging (OFDI) and μOCT, were compared to representative hematoxylin-eosin histology.

Results—Thyroid, fat, muscle, lymph nodes, and parathyroid tissues were evaluated. Histologic-like microscopic characteristics sufficient for tissue type identification was realized using both systems for all tissue types examined.

Conclusion—This pilot study demonstrated that new-generation OCT systems are capable of recognizing and differentiating neck tissues encountered during thyroid and parathyroid surgeries. Further advances in OCT miniaturization and development of sterile intraoperative probe formats may allow OCT to offer an intraoperative “optical biopsy” without fixation, staining, or tissue resection.

[*]**Corresponding author:** G. W. Randolph, Massachusetts Eye and Ear Infirmary, 243 Charles Street, Boston, MA 02114-3002. gregory_randolph@meei.harvard.edu.
Guillermo J. Tearney and Gregory W. Randolph contributed equally to this work.

Keywords

parathyroidectomy; thyroidectomy; thyroid cancer; parathyroid adenoma; hyperparathyroidism

INTRODUCTION

Many techniques have been proposed to reach an accurate preoperative diagnosis of thyroid, parathyroid, and metastatic lymph nodes lesions.[1–10] Nevertheless, intraoperative frozen-section examinations are frequently necessary to confirm or help in surgical decision-making. Traditionally, frozen-section analysis has been useful for examining atypical or suspicious thyroid nodules, for confirming lymph node malignant disease, and for diagnosing parathyroid pathologies, especially in evaluation of multiple gland disease. In addition, it is important when preserving parathyroid tissue during thyroid surgery (especially thyroid cancer surgery and central neck dissection) to distinguish parathyroid from adipose tissue, extra-thyroidal nodule, or malignant lymph nodes during surgery.

Unfortunately, frozen-section analysis is a time-consuming and expensive examination. Delays caused by frozen sections contribute to an increase in operative time and cost.[11] Also, frozen sections require that the examined tissue be removed from the patient. To define a tissue type through histologic examination, one must therefore sacrifice that tissue. Even limited biopsy with frozen section can be problematic in cases related to parathyroid gland identification, because it can be associated with hypoparathyroidism.[12]

Optical coherence tomography (OCT)[13] is a diagnostic method that is capable of obtaining histologic-like images from intact tissue surfaces without any tissue fixation or staining. OCT is similar to ultrasound imaging, except that it uses light rather than acoustic waves, which is associated with higher resolution. OCT was introduced as a method of noninvasive investigation of the human eye.[14] Recently, it has been used for characterization of lung, gastrointestinal, brain, coronary, and other tissues.[15–19] If OCT further evolves in terms of miniaturization and development of sterile probe formats, it could offer an “optical biopsy” of the parathyroid gland (as opposed to thyroid tissue/thyroid rest, fat, thymus, or lymph nodes) in situ without its removal, could open up a new empowering dynamic in parathyroid gland identification and preservation during thyroid cancer surgery.

In this pilot study, we evaluated the potential of OCT as a technique for determination of tissue type via immediate observation of fresh, nonstained, and surgically excised neck tissue. The purpose of this study was to investigate OCT images from thyroid or parathyroid surgery to provide a preliminary assessment as to whether these images contain sufficient microscopic information for identification and differentiation of different types of tissues encountered during these surgeries as compared to standard formal histologic evaluation.

MATERIALS AND METHODS

Two new-generation OCT systems, optical frequency domain imaging (OFDI)[20] and μOCT[21] were used to determine the architectural and cellular morphologic patterns of

normal neck specimens. Images were compared to conventional hematoxylin-eosin stained histology obtained from nearby locations in the same tissues.

Optical frequency-domain imaging

OFDI is a high-speed form of OCT that uses a narrow-band wavelength swept source, centered at 1310 nm, with a spectral bandwidth of approximately 100 nm. Spectral interference between light reflected from the specimen and a reference mirror is detected as the laser's wavelength is scanned. The spectral interference is Fourier transformed to obtain data representing reflectance as a function of depth within the tissue.[22–24] The specifications of the OFDI system used in this study have been previously published in detail.[25] Reflectance profiles as a function of depth (A-lines) were acquired at 62 kHz. The axial (depth) resolution of the OFDI system was 8 μm (in tissue; $n = 1.4$) and the OFDI probe optics provided a transverse resolution of approximately 30 μm. Three-dimensional images were acquired by scanning the sample arm beam in 2 dimensions, resulting in volume datasets comprising 1024 (axial) × 512 (transverse, x) × 512 (transverse, y) pixels over a field of view of 2.66 (height) × 2.66 (width) × 5.3 (depth) mm. The OFDI system acquired these 3D OCT datasets in 4.2 seconds.

μOptical coherence tomography

μOCT is a high-resolution form of OCT, defined by an axial resolution ≤1 μm and a transverse resolution ≤2 μm.[21] In this study, our μOCT system was based on spectral-domain OCT technology[20] that uses a broad bandwidth light source and a spectrometer to measure the spectral interference between the sample and a reference.[22,26–32] The μOCT system used in this study has been described elsewhere.[20] In brief, our system used a broad bandwidth source (300 nm) centered at 800 nm. The broad bandwidth of the light source provided an axial resolution of 1.0 μm (in tissue; $n = 1.4$). The transverse resolution was 2 μm. Cross-sectional images were acquired at a speed of 4 frames per second with 2000 A-lines per image. As with OFDI, we obtained 3-dimensional images by scanning the sample in 2 dimensions. The 3-dimensional field of view was 2 (height) × 2 (width) × 0.4 (depth) mm. Three-dimensional μOCT datasets were acquired in 8.3 minutes.

Specimens

Adult patients with existing thyroid or parathyroid disease undergoing surgical treatment were enrolled in this study. Imaging was performed on tissue collected during surgery. A small section of normal tissue was taken for experimental imaging purposes. Excised tissues were kept in phosphate-buffered saline and transported immediately to the Wellman Center of Photomedicine to be imaged by the OFDI and μOCT systems. The study protocol was approved by the Massachusetts Eye and Ear Infirmary Institutional Review Board.

Histologic analysis and registration

Immediately after imaging, samples were fixed in formalin. Samples were then processed, embedded in paraffin, cut into 5-μm thick slices, and stained using hematoxylin-eosin. For each sample, representative histologic sections were obtained from or adjacent to the imaged tissue regions and compared to cross-sectional or transverse (en face) μOCT and OFDI data.

The only modifications to the OFDI and μOCT images were averaging up to 3 adjacent frames to reduce speckle noise and adjustment of brightness and contrast.

RESULTS

The samples were collected from 25 patients (18 women and 7 men; age, 51.4 ± 11.6 years [mean ± SD]), undergoing thyroidectomy for benign disease (n = 11), thyroidectomy for malignant disease (n = 8), parathyroidectomy for adenoma (n = 5), neck dissection for thyroid cancer (n = 2), parathyroidectomy for hyperplasia (n = 1), or reoperation for recurrent malignant disease (n = 1). The tissue specimens included thyroid gland (n = 17), adipose tissue (n = 15), muscle (n = 15), lymph nodes (n = 9), and normal parathyroid gland (n = 5). Herein, we present representative examples of μOCT, OFDI, and histology for the different tissue types.

Thyroid gland

The thyroid gland is composed of spherical structural units called thyroid follicles, lined by simple cuboidal epithelium. Thyroid follicles are filled with a stored glycoprotein, thyroglobulin, seen as colloid, used in the thyroid hormone production process. Both OFDI and μOCT images from thyroid tissue show clear evidence of follicles, seen as multiple round structures with varying size (Figure 1). The central areas that have a low OCT signal represent the colloid. In some frames, the nuclei of thyroid epithelial cells can be seen lining the follicle. Within the follicle, there are some punctate, highly reflecting dots, which may represent dense colloid. Regions in between the follicles are filled by connective tissue. A capsule containing small vessels can be observed in some images (Figure 1).

Parathyroid gland

A normal parathyroid gland includes organized connective tissue septa that emanates from a delicate capsule over the gland that contains blood vessels. The parathyroid parenchyma is composed of chief cells, oxyphil cells, and adipocytes. Mature fat cells can be seen in the stromal compartment, sometimes present in clusters. These adipocytes were easily recognized in OFDI and μOCT as large dark ovoid or round structures (Figure 2). The remainder of the parathyroid parenchyma was homogeneous by OFDI and μOCT.

Adipose tissue

Adipose tissue is characterized by an accumulation of large numbers of adipocytes, surrounded by a fine network of reticular fibers. Each cell contains intracellular lipid and a thin rim of cytoplasm with a flattened nucleus. In histological preparation the lipid is removed, showing only a thin and delicate cell membrane envelope. Both OFDI and μOCT images showed dark areas representing intracellular lipid inclusions. Thicker areas that contained brighter dots may correspond with adipocyte nuclei (Figure 3). In the OCT images, the extracellular tissue contained thin lines of highly scattering tissue, possibly representing reticular fibers.

Muscle

Muscle fibers, separated by endomysium, were identified in both transverse and cross-sectional OFDI and μOCT images. In μOCT, fibers appeared as dark structures surrounded by a bright connective tissue that represents the endomysium, whereas in OFDI images they were visible in longitudinal views, as gray fascicles with a black background. The resolution of about 2 μm in μOCT allowed the visualization of small, highly scattering foci at the periphery of the fascicles (Figure 4), which likely represent nuclei of skeletal myocytes. The A, I, and Z-bands were not observed with either technology.

Lymph nodes

Lymph nodes are traditionally regarded as presenting 3 compartments, the cortex, paracortex, and medulla. The cortex contains spherical follicles that are surrounded and separated by interfollicular (or diffuse) cortex. There was a good correspondence between the μOCT and hematoxylin-eosin histology appearance of normal lymph nodes (Figure 5). The capsule was clearly identified by μOCT as a highly reflecting structure covering the lymph nodes. In addition, μOCT images showed evidence of follicles in the cortex as structures with slightly less backscattering and more heterogeneity than the perifollicular regions (Figure 5).

DISCUSSION

In this pilot study, we have demonstrated that 2 new-generation OCT technologies are capable of providing useful microscopic architectural information about tissue specimens obtained during thyroid and parathyroid surgery. The 3-dimensional capabilities of μOCT and OFDI allow visualization of the data in both cross-sectional and transverse formats, which further increases the diagnostic capabilities of these imaging methods. Further prospective studies must be conducted to determine the sensitivity and specificity of μOCT and OFDI for delineating different head and neck tissue types.

Examination of normal tissue during a surgical procedure is potentially very useful in thyroid and parathyroid surgery, mainly in parathyroid gland identification. After total thyroidectomy, temporary or definitive postoperative hypoparathyroidism occurs commonly, effecting 25% and 1% to 2%, respectively.[33–37] Postoperative hypoparathyroidism occurs as a result of parathyroid removal or ischemia, and may be directly related to the surgeon's capacity to detect and preserve the gland. This task is frequently difficult, because the parathyroid glands are commonly confused with lymph nodes, adipose tissue, or extraglandular thyroid tissue.

To our knowledge, this study provides the first description of the OCT imaging of the parathyroid gland. The ability to identify normal and pathologic features of the parathyroid gland can be very useful in many situations that require intraoperative decision-making for thyroid surgery as well as for parathyroid surgery. Primary hyperparathyroidism can be associated with single adenomas or multiple hyperplasic glands. Size and appearance of diseased glands may be quite close to normal glands, but are associated with reduced adipocyte content and increased cellularity.

The possibility of performing an optical biopsy using an OCT device would have widespread application in intraoperative investigation of neck nodal metastases.[38] The incidence of neck macrometastases from papillary thyroid carcinoma is about 35% of patients with the rate of micrometastasis as high as 80%.[39] Because of the current difficulty in diagnosing neck metastasis, recommendation regarding neck dissection is one of the most controversial issues in thyroid carcinoma treatment.

Both methods used in this study are very similar in the en face 2-dimensional field of view, but the OFDI system is faster and it permits imaging that is substantially deeper than μOCT. It would be very important to image areas in which the capsule of connective tissue is thicker. On the other hand, μOCT provides higher resolution than OFDI. A high-resolution image could be important for potentially recognizing neoplastic cells, a capability that will be investigated in further studies. A combined OFDI/μOCT system could possibly afford the best features in resolution, contrast, speed, penetration depth, and field of view.

The main limitation of this pilot study was that it was a preliminary descriptive study ex vivo. Furthermore, although histologic sections of the imaged tissues were obtained from adjacent regions for comparison, one-to-one registration was not achieved. Although it is far ready to supplant frozen section at this point, we believe this study provides a first step toward understanding the capabilities of these newer generation OCT technologies in head and neck tissue evaluation, meriting the conduct of prospective blinded, controlled studies to evaluate thyroid and parathyroid pathologies in the future. In the future studies with a handheld device, in vivo could further validate the technology and demonstrate its efficacy for surgeon decision-making in thyroid and parathyroid surgery.

Acknowledgments

We gratefully acknowledge the financial support from CAPES (Coordination for the Improvement of Higher Level – or education – Personnel) to Dr. Luiz C. Conti de Freitas, while in Boston, Massachusetts.

Contract grant sponsor: The National Institutes of Health; contract grant number: NIH R01 CA103769.

Author Disclosure Statement: Guillermo J. Tearney receives consulting income and nonclinical sponsored research support from Ninepoint Medical. Massachusetts General Hospital and Ninepoint Medical have a licensing arrangement regarding the optical frequency domain imaging technology. Dr. Tearney has the right to receive royalties from this licensing arrangement. Eman Namati has been employed and owns stock at NinePoint Medical Inc. Cambridge, Massachusetts.

References

1. Mangano JJ. Geographic variation in U.S. thyroid cancer incidence and a cluster near nuclear reactors in New Jersey, New York, and Pennsylvania. Int J Health Serv. 2009; 39:643–661. [PubMed: 19927407]
2. Menegaux F, Turpin G, Dahman M, et al. Secondary thyroidectomy in patients with prior thyroid surgery for benign disease: a study of 203 cases. Surgery. 1999; 126:479–483. [PubMed: 10486599]
3. Khan AA, Bilezikian JP, Potts JT Jr, Guest Editors for the Third International Workshop on Asymptomatic Primary Hyperparathyroidism. The diagnosis and management of asymptomatic primary hyperparathyroidism revisited. J Clin Endocrinol Metab. 2009; 94:333–334. [PubMed: 19193907]

4. Eastell R, Arnold A, Brandi ML, et al. Diagnosis of asymptomatic primary hyperparathyroidism: proceedings of the third international workshop. J Clin Endocrinol Metab. 2009; 94:340–350. [PubMed: 19193909]
5. Uhlig K, Berns JS, Kestenbaum B, et al. KDOQI US commentary on the 2009 KDIGO clinical practice guideline for the diagnosis, evaluation, and treatment of CKD-mineral and bone disorder (CKD-MBD). Am J Kidney Dis. 2010; 55:773–799. [PubMed: 20363541]
6. Varcus F, Peix JL, Berger N, Bordos D. Thyroid scintigraphy: its place in preoperative diagnosis of thyroid nodules?Article in French. Ann Chir. 2002; 127:685–689. [PubMed: 12658827]
7. Peccin S, de Castsro JA, Furlanetto TW, Furtado AP, Brasil BA, Czepielewski MA. Ultrasonography: is it useful in the diagnosis of cancer in thyroid nodules? J Endocrinol Invest. 2002; 25:39–43. [PubMed: 11885575]
8. Hwang HS, Perez DA, Orloff LA. Comparison of positron emission tomography/computed tomography imaging and ultrasound in staging and surveillance of head and neck and thyroid cancer. Laryngoscope. 2009; 119:1958–1965. [PubMed: 19688854]
9. Cibas ES, Alexander EK, Benson CB, et al. Indications for thyroid FNA and pre-FNA requirements: a synopsis of the National Cancer Institute Thyroid Fine-Needle Aspiration State of the Science Conference. Diagn Cytopathol. 2008; 36:390–399. [PubMed: 18478607]
10. Chaudhary V, Bano S. Imaging of the thyroid: recent advances. Indian J Endocrinol Metab. 2012; 16:371–376. [PubMed: 22629501]
11. Lai P, Segall L, de Korompay N, Witterick I, Freeman J. Cost analysis of intraoperative frozen section examinations in thyroid surgery in a Canadian tertiary center. J Otolaryngol Head Neck Surg. 2009; 38:559–563. [PubMed: 19769826]
12. Cavicchi O, Piccin O, Caliceti U, De Cataldis A, Pasquali R, Ceroni AR. Transient hypoparathyroidism following thyroidectomy: a prospective study and multivariate analysis of 604 consecutive patients. Otolaryngol Head Neck Surg. 2007; 137:654–658. [PubMed: 17903586]
13. Huang D, Swanson EA, Lin CP, et al. Optical coherence tomography. Science. 1991; 254:1178–1181. [PubMed: 1957169]
14. Fercher AF, Hitzenberger CK, Drexler W, Kamp G, Sattmann H. In vivo optical coherence tomography. Am J Ophthalmol. 1993; 116:113–114. [PubMed: 8328536]
15. Aguirre AD, Chen Y, Bryan B, et al. Cellular resolution ex vivo imaging of gastrointestinal tissues with optical coherence microscopy. J Biomed Opt. 2010; 15:016025. [PubMed: 20210470]
16. Michel RG, Kinasewitz GT, Fung KM, Keddissi JI. Optical coherence tomography as an adjunct to flexible bronchoscopy in the diagnosis of lung cancer: a pilot study. Chest. 2010; 138:984–988. [PubMed: 20472863]
17. Low AF, Kawase Y, Chan YH, Tearney GJ, Bouma BE, Jang IK. In vivo characterisation of coronary plaques with conventional grey-scale intravascular ultrasound: correlation with optical coherence tomography. EuroIntervention. 2009; 4:626–632. [PubMed: 19378684]
18. Vakoc BJ, Lanning RM, Tyrrell JA, et al. Three-dimensional microscopy of the tumor microenvironment in vivo using optical frequency domain imaging. Nat Med. 2009; 15:1219–1223. [PubMed: 19749772]
19. Chia S, Raffel OC, Takano M, Tearney GJ, Bouma BE, Jang IK. Comparison of coronary plaque characteristics between diabetic and non-diabetic subjects: an in vivo optical coherence tomography study. Diabetes Res Clin Pract. 2008; 81:155–160. [PubMed: 18455829]
20. Bouma BE, Yun SH, Vakoc BJ, Suter MJ, Tearney GJ. Fourier-domain optical coherence tomography: recent advances toward clinical utility. Curr Opin Biotechnol. 2009; 20:111–118. [PubMed: 19264475]
21. Liu L, Gardecki JA, Nadkarni SK, et al. Imaging the subcellular structure of human coronary atherosclerosis using micro-optical coherence tomography. Nat Med. 2011; 17:1010–1014. [PubMed: 21743452]
22. Yun S, Tearney G, Bouma B, Park B, de Boer J. High-speed spectral-domain optical coherence tomography at 1.3 mum wavelength. Opt Express. 2003; 11:3598–3604. [PubMed: 19471496]
23. Choma M, Sarunic M, Yang C, Izatt J. Sensitivity advantage of swept source and Fourier domain optical coherence tomography. Opt Express. 2003; 11:2183–2189. [PubMed: 19466106]

24. Golubovic B, Bouma BE, Tearney GJ, Fujimoto JG. Optical frequency-domain reflectometry using rapid wavelength tuning of a Cr4+:forsterite laser. Opt Lett. 1997; 22:1704–1706. [PubMed: 18188341]
25. Yun S, Tearney G, de Boer J, Iftimia N, Bouma B. High-speed optical frequency-domain imaging. Opt Express. 2003; 11:2953–2963. [PubMed: 19471415]
26. Cense B, Nassif N, Chen T, et al. Ultrahigh-resolution high-speed retinal imaging using spectral-domain optical coherence tomography. Opt Express. 2004; 12:2435–2447. [PubMed: 19475080]
27. Leitgeb RA, Drexler W, Unterhuber A, et al. Ultrahigh resolution Fourier domain optical coherence tomography. Opt Express. 2004; 12:2156–2165. [PubMed: 19475051]
28. Wojtkowski M, Srinivasan VJ, Ko TH, Fujimoto JG, Kowalczyk A, Duker J. Ultrahigh-resolution, high-speed, Fourier domain optical coherence tomography and methods for dispersion compensation. Opt Express. 2004; 12:2404–2422. [PubMed: 19475077]
29. Choma M, Sarunic M, Yang C, Izatt J. Sensitivity advantage of swept source and Fourier domain optical coherence tomography. Opt Express. 2003; 11:2183–2189. [PubMed: 19466106]
30. de Boer JF, Cense B, Park BH, Pierce MC, Tearney GJ, Bouma BE. Improved signal-to-noise ratio in spectral-domain compared with time-domain optical coherence tomography. Opt Lett. 2003; 28:2067–2069. [PubMed: 14587817]
31. Nassif N, Cense B, Park BH, et al. In vivo human retinal imaging by ultrahigh-speed spectral domain optical coherence tomography. Opt Lett. 2004; 29:480–482. [PubMed: 15005199]
32. Ha Usler G, Lindner MW. “Coherence radar” and “spectral radar”—new tools for dermatological diagnosis. J Biomed Opt. 1998; 3:21–31. [PubMed: 23015002]
33. Asari R, Passler C, Kaczirek K, Scheuba C, Niederle B. Hypoparathyroidism after total thyroidectomy: a prospective study. Arch Surg. 2008; 143:132–137. discussion 138. [PubMed: 18283137]
34. American Thyroid Association (ATA) Guidelines Taskforce on Thyroid Nodules and Differentiated Thyroid Cancer. Cooper DS, Doherty GM, et al. Revised American Thyroid Association management guidelines for patients with thyroid nodules and differentiated thyroid cancer. Thyroid. 2009; 19:1167–1214. [PubMed: 19860577]
35. Pantanowitz L, Hsiung PL, Ko TH, et al. High-resolution imaging of the thyroid gland using optical coherence tomography. Head Neck. 2004; 26:425–434. [PubMed: 15122659]
36. Zhou C, Wang Y, Aguirre AD, et al. Ex vivo imaging of human thyroid pathology using integrated optical coherence tomography and optical coherence microscopy. J Biomed Opt. 2010; 15:016001. [PubMed: 20210448]
37. Ishida S, Nishizawa N. Ex-vivo imaging of thyroid gland using ultrahigh-resolution optical coherence tomography at wavelength from 800 to 1700 nm. Jpn J Appl Phys. 2012; 51:030203.
38. McLaughlin RA, Scolaro L, Robbins P, Hamza S, Saunders C, Sampson DD. Imaging of human lymph nodes using optical coherence tomography: potential for staging cancer. Cancer Res. 2010; 70:2579–2584. [PubMed: 20233873]
39. Randolph GW, Duh QY, Heller KS, et al. The prognostic significance of nodal metastases from papillary thyroid carcinoma can be stratified based on the size and number of metastatic lymph nodes, as well as the presence of extranodal extension. Thyroid. 2012; 22:1144–1152. [PubMed: 23083442]

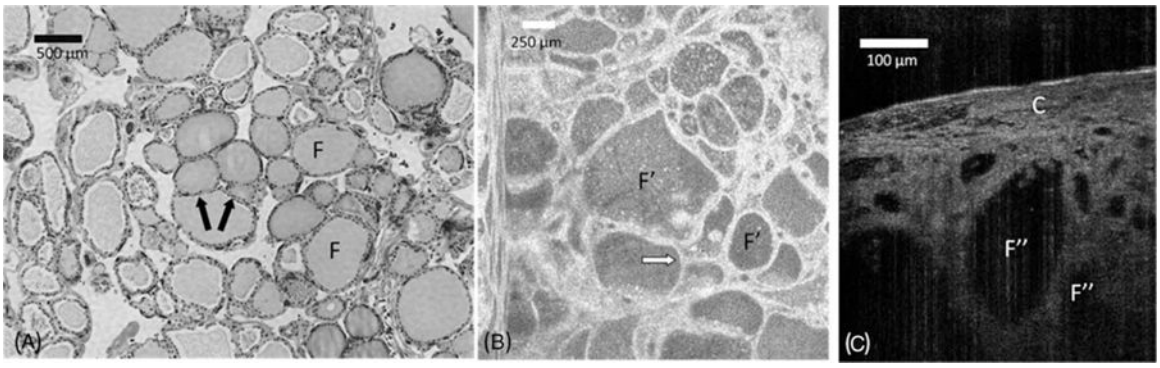

FIGURE 1.

Comparison between (A) hematoxylin-eosin slides (original magnification ×40), (B) en face optical frequency domain imaging (OFDI), and (C) cross-sectional µ-optical coherence tomography (µOCT) images of normal thyroid gland. The thyroid gland shows spherical structural units – thyroid follicles (F), which include simple cuboidal epithelium that lines these structures (arrows). OFDI and µOCT images show multiple thyroid follicles (F′ and F ″, respectively). A capsule of connective tissue with some small vessels can be observed in a cross-sectional µOCT view (C).

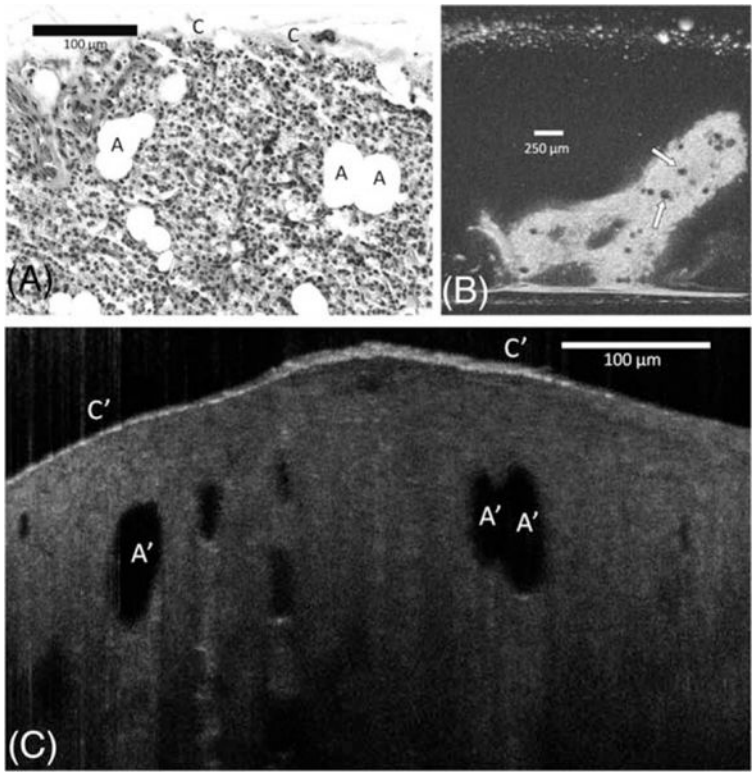

FIGURE 2.

Comparison between (A) hematoxylin-eosin slides (original magnification ×100), (B) en face optical frequency domain imaging (OFDI), and (C) cross-sectional μ-optical coherence tomography (μOCT) images of the normal parathyroid gland. The gland is covered by a delicate capsule (C); its parenchyma is composed by chief cells, oncocyte cells, and adipose cells (A). Adipocytes are easily recognized in OFDI (arrows) and μOCT as a large dark ovoid or round shaped structures (A′). A thin but bright capsule covers the glandular parenchyma (C′).

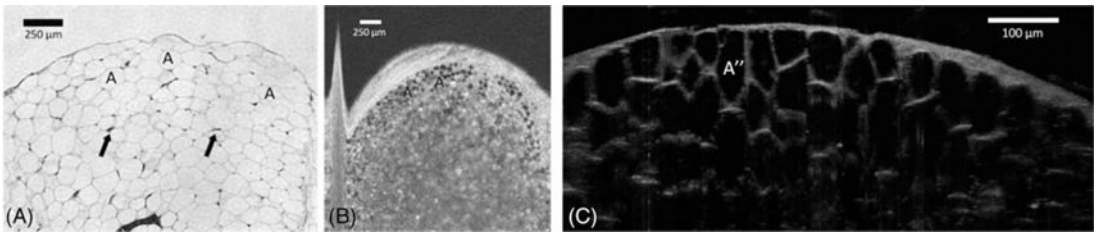

FIGURE 3.

Comparison between (A) hematoxylin-eosin slides (original magnification ×100), (B) en face optical frequency domain imaging (OFDI), and (C) cross-sectional µ-optical coherence tomography (µOCT) images of adipose tissue. Adipose tissue demonstrates a dense collection of adipocytes (A) with flattened nuclei (arrows), surrounded by a fine network of reticular fibers. Both OFDI and µOCT show areas of low reflectance representing lipid inclusions (A′ and A″, respectively). The area between lipid inclusions comprise thin and highly reflecting lines that are consistent with reticular fibers or cell walls.

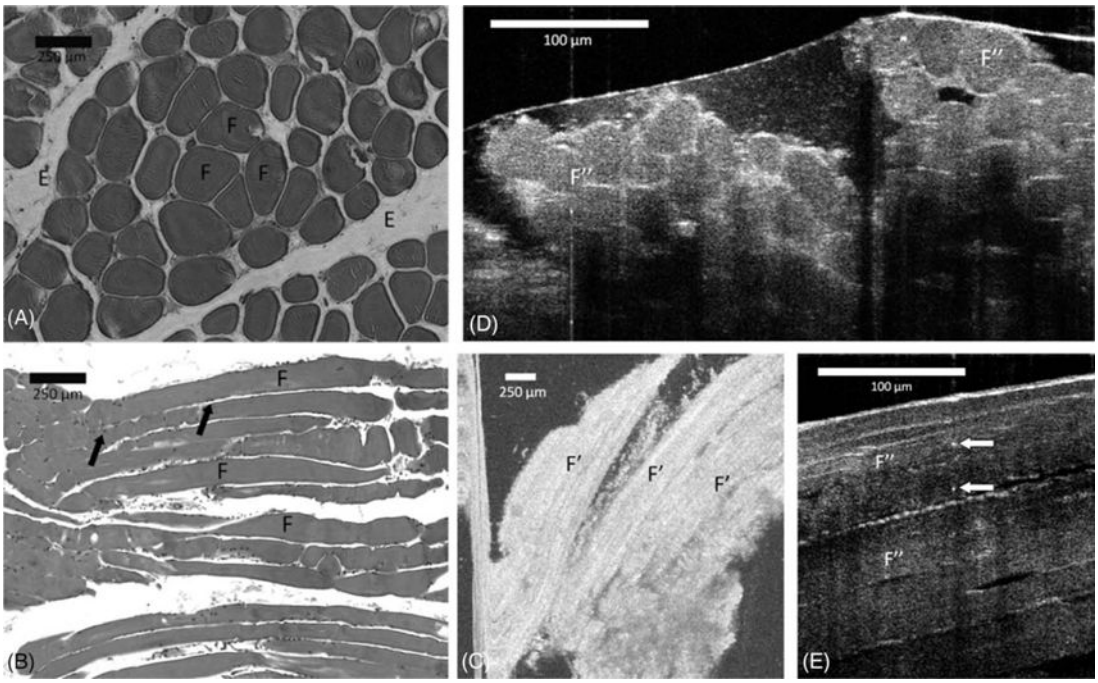

FIGURE 4.

Comparison between (A) transverse and (B) longitudinal section hematoxylin-eosin slides (original magnification ×100), (C) en face optical frequency domain imaging (OFDI), and cross-sectional μ-optical coherence tomography (μOCT) images of (D) transverse and (E) longitudinal view of muscle tissue. Skeletal muscle fibers occur in bundles (F), separated by endomysium (E). The myocyte nuclei are located peripherally within the bundle (arrows). In the OFDI image, the myocytes appear in the longitudinal view as elongated gray bands against a black background (F′). μOCT image demonstrates fascicles (F″) surrounded by endomysium. Bright dots that possibly represent nuclei (white arrows) can be recognized in the μOCT image.

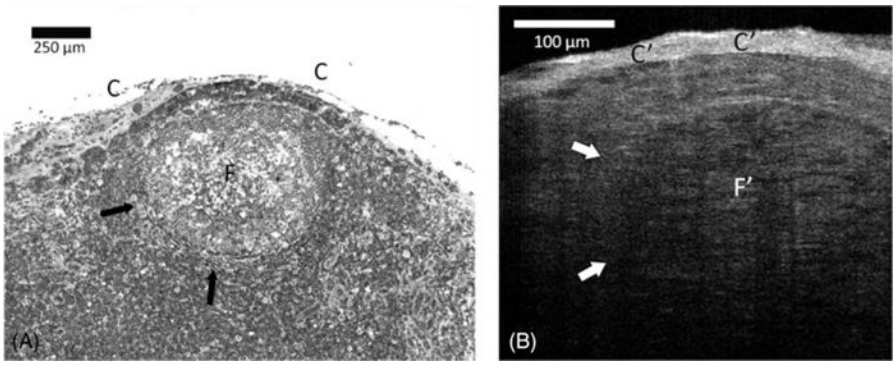

FIGURE 5.

Comparison between (A) hematoxylin-eosin slides (original magnification ×100) and (B) cross-sectional µ-optical coherence tomography (µOCT) images of lymph nodes. A clear capsule (C) has a high µOCT signal (C′). A large well-delineated (F) and less dense round subcapsular structure (arrows) corresponding to a lymphoid follicle can be recognized in the µOCT image (F′).